RSC Advances

ROYAL SOCIETY OF CHEMISTRY

www.rsc.org/advances

RSC Advances

ARTICLE

Mesoporous ZnZSM-5 Zeolites Synthesized by One-Step Desilication and Reassembly: Durable Catalyst for Methanol Aromatization

Received 00th January 20xx,
Accepted 00th January 20xx

DOI: 10.1039/x0xx00000x

www.rsc.org/

Xiaoxing Wang [a], Junfeng Zhang [a], Tao Zhang [a], He Xiao [a], Faen Song [a], Yizhuo Han [a] and Yisheng Tan [a,b,*]

Mesoporous ZnZSM-5 zeolites were synthesized by introducing zinc directly into an alkaline and surfactant solution. The characterizations reveal that the presence of CTAB is favorable for the recrystallization of zeolite structural units. The amount of strong acid sites of mesoporous zeolites decreased, while the amount of medium acid sites of mesoporous zeolites (especial zinc-containing) increased. The amount of Lewis acid sites increased while the amount of Brønsted acid sites obviously decreased. For mesoporous ZnZSM-5, the emergence of a new species ($ZnOH^+$) further increased the amount of Lewis acid sites. Both the external surface area and mesopore volume of mesoporous ZnZSM-5 gradually decreased with increasing zinc content. Most of zinc species introduced during desilication and reassembly dispersed on the surface of zeolites, but the addition of zinc species had no obvious influence on the zeolite morphology. The catalytic performance of the obtained materials was investigated via aromatization of methanol. The results show that BTX (benzene, toluene, and xylene) selectivity over mesoporous ZnZSM-5 gradually increases with increasing zinc content, and is much higher than that of mesoporous HZSM-5. However, the BTX selectivity of mesoporous HZSM-5 is obviously lower than that of HZSM-5 due to its much lower strong acid sites and larger pore size. The strong Brønsted acid sites, the Zn-Lewis acid sites and mesoporous channels have a synergistic effect on methanol aromatization over mesoporous ZnZSM-5 catalysts. Additionally, compared with HZSM-5, improvement in catalyst lifetime of MHZSM-5 and MZnZSM-5-2 is achieved by introducing additional mesoporous channels and decreasing the amount of strong acid sites.

Introduction

Aromatics like benzene, toluene, and xylene (collectively abbreviated as BTX) are important raw materials in the organic chemical industry, and are widely used in polyester fibers, medicines, pesticides, and dyes. At present, almost all aromatics are derived from crude oil using industrial processes such as reforming, cracking, and alkylation.[1] However, with the exhaustion of petroleum resources, finding new processes to produce BTX light aromatics to replace processes using crude oil has important practical significance. So far, the route for BTX production from methanol via aromatization is regarded to be remarkably promising and also attracting researchers' interests. As is well-known, methanol is usually produced from syngas, which is formed by steam reforming of natural gas or gasification of coal and biomass, and is therefore abundantly available. Multiple catalytic processes have been developed to convert surplus methanol to high value-added fuels and chemicals such as gasoline, olefins, aromatics, and so on.[2–5]

ZSM-5 zeolite is commonly used for methanol aromatization as well as other catalytic processes (alkylation of toluene and methanol, disproportionation of toluene, conversion of methanol to hydrocarbons, *etc.*).[2,6] However, single ZSM-5 zeolite has poor activity and stability. Generally, some modification to ZSM-5 zeolite is needed to be done in order to gain the improved performance in methanol aromatization through introducing some metal species such as Ag、Cu、Cu/Zn、Ga_2O_3、Zn、La/Zn. [7–14] As reported, Ag-ZSM-5 zeolite was very active at initial reaction, but deactivated very rapidly because Ag^+ ions easily turned into Ag metal in the reductive atmosphere. [7,8] Zaidi found the high selectivity of aromatics on Cu/HZSM-5 catalyst in MTA, but the selectivity of BTX was not satisfactory and many carbon oxides were formed.[9] Barthos *et al.* reported that Mo_2C/ZSM-5 markedly enhanced the formation of aromatics at the expense of C_2-C_4 alkenes in the reaction, but this was mainly due to the dramatically enhanced

[a] *State Key Laboratory of Coal Conversion, Institute of Coal Chemistry, Chinese Academy of Sciences, Taiyuan 030001, China*
[b] *National Engineering Research Center for Coal-Based Synthesis, Institute of Coal Chemistry, Chinese Academy of Sciences, Taiyuan 030001, China*

**Corresponding author. Tel./Fax: +86-351-4044287. E-mail address: tan@sxicc.ac.cn.*

formation of C_9^+ aromatics.[11] Ono *et al.* investigated the aromatization performance of Zn^{2+} or Ga^{3+} exchanged ZSM-5 zeolite. A significantly improvement was observed from the catalyst test.[13] So far, the Zn-ZSM-5 catalyst exhibited the highest initial selectivity of BTX compared with those published works previously mentioned. Moreover, zinc species is the most commonly modified metal for the aromatization of methanol due to its advantageous dehydrogenation capability, low-cost and low-toxicity.[15,16]

Although ZSM-5 zeolite as an optional catalysis material indeed presents multiple supreme advantages, its drawbacks are also apparent. ZSM-5 zeolite usually suffers from intracrystalline diffusion limitation arising from its small micropores, and it is difficult for molecules with diameters larger than the pore openings to enter and approach the active sites, leading to limitations in its activity and durability. Considerable effort has been devoted to resolving the diffusion limitation imposed by zeolitic structures. The methods have mainly focused on preparing nanosized ZSM-5 or introducing intracrystalline hierarchical mesopores into zeolite crystals, which decreases the contact time of reaction intermediates. Various templates have been used to introduce mesopores or macropores into zeolite crystals, such as carbon particles, organic aerogels, polymers, and nanosized $CaCO_3$.[17–23] Conventional desilication of zeolites in basic media is simple and efficient, but this method has some negative effects on the pore structure and active sites of zeolites.[24,25] In recent years, researchers have developed another method to alleviate the above-mentioned limitation, in which mesoporosity is generated through dissolution and reassembly of amorphous silica directed by surfactant molecules.[26–30] Schmidt *et al.* reported a similar synthesis route, and the mesoporous zeolite showed improved catalyst stability in methanol to hydrocarbon converstion.[31] Furthermore, Al-Yassir *et al.* synthesized ordered mesoporous H-galloaluminosilicates by surfactant-mediated base hydrolysis and investigated application to propane aromatization.[32] Despite well-documented reports of the success of these strategies in improving the catalytic activity and lifetime, studies on aromatization of methanol over mesoporous zinc-containing ZSM-5 zeolite (MZnZSM-5) are still lacking.

In this study, a series of mesoporous ZnZSM-5 zeolites were synthesized by introducing Zn species into the process of alkaline desilication and surfactant-directed reassembly. The acidity, pore structure, chemical state of zinc species, morphology, and catalytic performance of mesoporous ZnZSM-5 were investigated by various characterization techniques and the aromatization of methanol reaction. The effect of the zinc content of mesoporous ZnZSM-5 on the aromatization of methanol, and the stabilities of mesoporous HZSM-5 (MHZSM-5) and MZnZSM-5 were investigated.

Experimental

Materials

Cetyltrimethylammonium bromide (CTAB) was purchased from Tianjin Fuchen Chemical Co., Ltd (Tianjin, China). Sodium hydroxide (NaOH) and ammonium nitrate (NH_4NO_3) were purchased from Tianjin Fengchuan Chemical Co., Ltd. (Tianjin, China). Zinc nitrate ($Zn(NO_3)_2{\cdot}6H_2O$) was purchased from Tianjin Tianda Chemical Co. Ltd. (Tianjin, China) and HZSM-5 (SiO_2/Al_2O_3 = 38) was purchased from NanKai University Catalyst Co. Ltd. (Tianjin, China). All materials were used without further purification.

Catalyst preparation

MHZSM-5 zeolite was synthesized according to a previously reported method.[31] Typically, 3.71 g CTAB was dissolved in an alkaline solution of 196 g H_2O and 4 g NaOH, and then HZSM-5 zeolite was dispersed in the above solution. The resulting mixture was vigorously stirred for desilication and reassembly at 80 °C for 24 h. The solution was then collected by filtration, washed, dried at 80 °C, and calcined at 550 °C for 6 h to remove the surfactant. After the obtained powder was treated three times with 0.4 M NH_4NO_3 solution at 80 °C (according to the ratio of 20 mL solution/g zeolite), MHZSM-5 zeolite was obtained.

Synthesis of MZnZSM-5 was similar to that of MHZSM-5. The difference was that 0.23 g (x = 1), 0.69 g (x = 2), or 1.15 g (x = 3) of $Zn(NO_3)_2{\cdot}6H_2O$ and 12 g of H_2O solution was added dropwise into the NaOH and CTAB mixture. The following synthesis steps were the same as those for MHZSM-5. MZnZSM-5 samples with different zinc contents were obtained: MZnZSM-5-x (where x = 1, 2, or 3, referring to the zinc content specified above). Preparation of MHZSM-5(NC) and MZnZSM-5-2(NC), where NC indicates no CTAB, was similar to that for MHZSM-5 and MZnZSM-5-2, respectively, except for the absence of CTAB.

Characterization

X-ray diffraction (XRD) patterns were recorded on a D8 Advance diffractometer using Cu Kα radiation at 40 kV and 100 mA. NH_3-temperature programmed desorption (NH_3-TPD) profiles were obtained using a TP-5080 chemisorption instrument. Typically, the catalyst (100 mg) was pretreated at 600 °C under N_2 flow (30 ml min^{-1}) for 0.5 h and then cooled to 100 °C to adsorb NH_3. The TPD profiles were recorded from 100 to 600 °C at a heating rate of 10 °C/min. Fourier transform infrared spectra of pyridine adsorption were recorded using a Thermo Nicolet Nexus spectrometer equipped with a liquid-nitrogen-cooled mercury–cadmium–telluride detector. Wafers of the samples were pretreated at 400 °C for 2 h in vacuum. After cooling, the samples were exposed to pyridine vapor at 40 °C. The excess pyridine was removed at 150 °C for 1 h under the vacuum, and the Py-IR spectra were collected after the temperature reduced to room temperature. The system was also evacuated at 350 °C, and IR spectra were recorded. The zinc contents and SiO_2/Al_2O_3 ratios of the as-prepared samples were determined on a Thermo ICAP 6300 inductively coupled plasma (ICP) emission spectrometer. N_2 adsorption–desorption isotherms were measured using a Micromeritics Tristar 3000 physical adsorption apparatus at 77 K. The samples were outgassed in vacuum at 350 °C for 4 h before the measurements. The specific surface area and pore size distribution were calculated using the Brunauer–Emmett–Teller (BET) method and Barrett–Joyner–Halenda (BJH) desorption branch, respectively. The external surface area, micropore surface area, and micropore volume were obtained by the *t*-plot method. The total pore volume was estimated from the amount of N_2 adsorbed at a relative

RSC Advances

ARTICLE

pressure P/P_0 = 0.99. X-ray photoelectron spectroscopy (XPS) was conducted on a Kratos company Axis Ultra DLD spectrometer with an Al Kα radiation source (1486.6 eV) and the XPS peaks were internally referenced to the binding energy of the C 1s peak at 284.8 eV. Scanning electron microscopy (SEM) images were obtained using a JSM-7001F scanning electron microscope. Transmission electron microscopy (TEM) images were obtained using a JEM-2010 high-resolution transmission electron microscope. The specimens were prepared by first dispersing the zeolite in ethanol by supersonic waves and then placing a drop onto a carbon-coated copper grid.

Catalytic tests

The methanol aromatization experiments were performed in a fixed-bed stainless steel reactor. Crushed and sieved (20–40 mesh) catalyst (1.86 g) was mixed with inert ceramic particles (5.7 g) of the same size. Before introduction of the feedstock, the catalyst bed was activated in pure nitrogen at 430 °C overnight. The feed liquid of methanol was then introduced using a calibrated syringe pump after shutting off N_2, and the products were recovered in a condenser. All of the experiments were carried out under atmospheric pressure. The gas products were analyzed by three gas chromatographs: one equipped with a carbon molecular sieve column and a thermal conductivity detector (TCD), one equipped with a GDX-401 column and a flame ionization detector (FID), and one equipped with an Al_2O_3 column and an FID. The results were calibrated by the methane concentration. The collected liquid oil species were analyzed using a gas chromatograph equipped with a RTX-1 capillary column (60 m × 0.25 mm) and an FID, and the aqueous products were analyzed by a gas chromatograph with a GDX-403 column and a TCD. The conversion of methanol and the selectivity of different products are the conversion and molar selectivity of carbon atoms, respectively.

Results and discussion

Catalyst characterization

Fig. 1 shows XRD patterns of the as-prepared samples. In Fig. 1(a), all of the samples exhibit the typical peaks of the MFI structure in the range 2ϑ = 5–40°. No diffraction peaks of ZnO crystallites (2ϑ = 31.6°, 34.2°, 36.1°, 56.6°) are observed in the MZnZSM-5-*x* samples in the range 2ϑ = 30–80°, indicating that the zinc species are highly dispersed in zeolites or amorphous zinc species are formed. [15,16] Chen *et al.* revealed that the diffraction peaks of ZnO are not observed in XRD patterns when its loading is below 4wt%.[33] MHZSM-5 is slightly less crystalline, showing that alkaline desilication and CTAB-mediated reassembly does not lead to severe

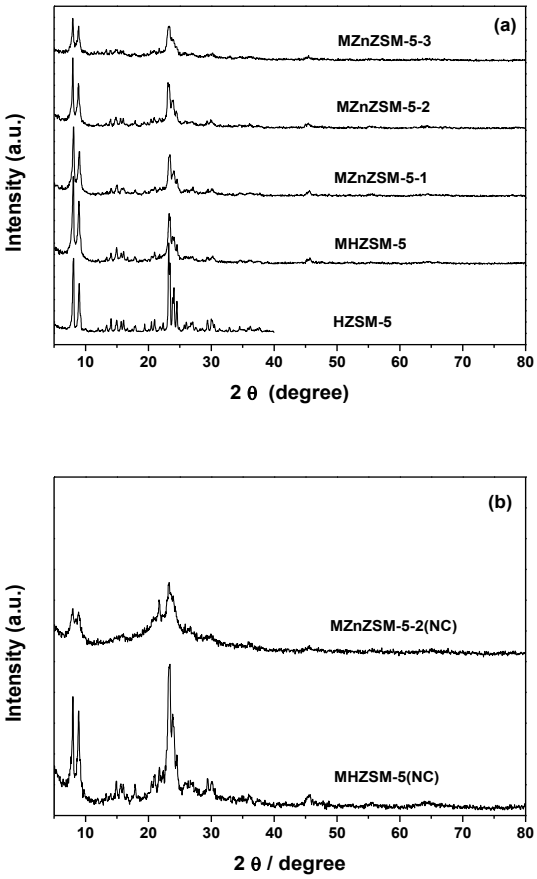

Fig. 1. XRD patterns of (a) HZSM-5, MHZSM-5, and MZnZSM-5-x, (b) MHZSM-5(NC), and MZnZSM-5-2(NC) samples.

destruction of the zeolite structure. The crystallinity of the MZnZSM-5-*x* samples gradually decreases with increasing zinc content, suggesting that the introduction of zinc species affects the crystallization of MZnZSM-5-*x*. In addition, MHZSM-5(NC) and MZnZSM-5-2(NC) samples were prepared to further justify the reassembly process (Fig. 1(b)). MHZSM-5(NC) and MZnZSM-5-2(NC) have lower crystallinity than MHZSM-5 and MZnZSM-5-2, especially MZnZSM-5-2(NC), which has extremely poor crystallinity. This indicates that the dissolved zeolite structural units did not assemble very well, and zinc species affect the crystallization of MZnZSM-5-2(NC) seriously. It is plausible that the introduction of CTAB to the parent solution is favorable for reconstructing the zeolite structure.The five diffraction peak intensities of HZSM-5 were assumed to be 100 % crystallinity, and the relative crystallinities of different samples were shown in Table 1. MHZSM-5 and MZnZSM-5-2 exhibit higher yields than MHZSM-5(NC) and MZnZSM-5-2(NC) respectively, which further confirms the reassemble process of

RSC Advances

ARTICLE

Table 1 Bulk and surface compositions of the different samples.

Sample	Crystallization (%)	Yield (%)	SiO_2/Al_2O_3[a] (molar ratio)	SiO_2/Al_2O_3[b] (molar ratio)	Zn[a] (wt.%)	Zn[b] (atom ratio)	Si/Zn[a] (molar ratio)	Si/Zn[b] (molar ratio)
HZSM-5	100	--	38.5	--	--	--	--	--
MHZSM-5	87	35	20.7	--	--	--	--	--
MZnZSM-5-1	71	41	22.4	18.6	0.09	0.23	1082.1	80.7
MZnZSM-5-2	74	52	24.3	19.6	1.58	1.47	61.8	12.5
MZnZSM-5-3	53	53	22.3	20.6	3.11	2.32	30.2	8.8
MHZSM-5(NC)	54	32	16.0	--	--	--	--	--
MZnZSM-5-2(NC)	29	41	17.4	16.0	2.74	1.10	33.7	20.7

[a]Bulk content by ICP analysis.
[b]Surface content by XPS analysis.

zeolite structural units with CTAB, similar results were reported in the literature.[31] Furthermore, the SiO_2/Al_2O_3 ratio of MHZSM-5 is approximately half that of the parent HZSM-5 sample, whereas the SiO_2/Al_2O_3 ratios of the MZnZSM-5-*x* samples are slightly higher by ICP (Table 1). This is ascribed to that the addition of zinc hinders silicon extraction. This viewpoint is confirmed by the gradually increasing yields of the MZnZSM-5-*x* samples with increasing zinc content. The bulk Zn and surface Zn atom contents of MZnZSM-5-*x* increase with the increase of zinc content by ICP and XPS. However, the surface Si/Zn ratios of MZnZSM-5-x are obviously lower than ones of the bulk, suggesting that the introduced zinc species preferentially disperse on the surface of MZnZSM-5-x samples. In addition, it can be observed that the surface Si/Zn ratio of MZnZSM-5-2(NC) is much higher than that of MZnZSM-5-3 based on their similar bulk Si/Zn ratios althogh MZnZSM-5-2(NC) also shows the lower surface Si/Zn ratio than the bulk. These results indicate that zinc species in MZnZSM-5-2(NC) and MZnZSM-5-x disperse different obviously due to their different pore structure.

Fig. 2 shows NH_3-TPD profiles of the as-prepared samples. Generally, two desorption peaks are observed for HZSM-5 zeolite: a low-temperature peak at about 200 °C and a high-temperature peak in the range of 370–400 °C. [16] The area of desorption peak measures the amount of acid sites and the temperature of desorption peak reflects the acid strength of the sample.[34] In our work, the introduction of zinc species on MHZSM-5 zeolite obviously broaden the low-temperature desorption peak. Therefore, the distributions of acid sites by integrating the NH_3-TPD profiles in three desorption peaks (vertex about 220 °C, 290 °C and 400 or 460 °C). Usually, the weak acid sites are inactive in MTH reactions.[35] Thus, we mainly focus on the changes on the medium and strong acid sites. Compared with HZSM-5, the intensity of high-temperature desorption peak of MHZSM-5 is lower and the peak

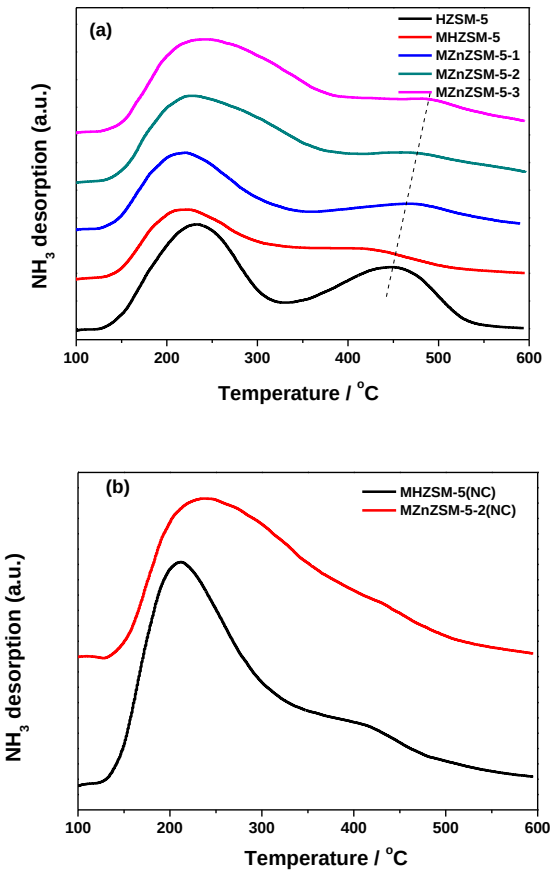

Fig. 2. NH_3-TPD profiles of (a) HZSM-5, MHZSM-5, and MZnZSM-5-x, (b) MHZSM-5(NC), and MZnZSM-5-2(NC) samples.

Table 2 Peak areas integrated from NH_3-TPD profiles of the different samples.

Samples	Total acid sites[a] (μmol/g)	Weak acid sites[b] (μmol/g)	Medium acid sites[b] (μmol/g)	Strong acid sites[b] (μmol/g))
HZSM-5	561.8	319.4	38.4	204.1
MHZSM-5	340.9	155.9	51.7	133.3
MZnZSM-5-1	339.9	167.3	73.3	99.2
MZnZSM-5-2	440.7	147.4	184.3	109.0
MZnZSM-5-3	499.7	120.7	268.1	110.9
MHZSM-5(NC)	355.3	174.7	75.6	105.0
MZnZSM-5-2(NC)	320.0	76.9	167.3	75.8

[a] Determined by NH_3-TPD.
[b] Quantified by deconvolution of the NH_3-TPD profiles with Gaussian peaks (R^2> 0.99).

position is at lower temperature, indicating that the amount and strength of strong acid sites are lower. This is attributed to the obvious decrease of Si(OH)Al sites (Brønsted acid sites) due to the dissolution of silica framework. The introduction of zinc species in MHZSM-5 exhibits a significant influence on the distribution and amount of acid sites. The area of medium-temperature desorption peak of MZnZSM-5-*x* gradually increases with increasing zinc content, and meanwhile the temperature of high-temperature desorption peak enhances (Fig. 2(a)), suggesting that the amount of medium acid sites increases and the strength of strong acid sites enhances after the introduction of zinc species. For the catalysts without the addition of CTAB (MHZSM-5(NC) and MZnZSM-5-2(NC)), the intensities of the high-temperature desorption peaks are much lower than those of the catalysts with addition of CTAB (Fig. 2(b)). In addition, the amounts of weak, medium, and strong acid sites were calculated and are listed in Table 2. Compared with HZSM-5 and MHZSM-5, the amounts of medium acid sites are increased markedly in the MZnZSM-5-x samples at the expense of the strong and weak acid sites due to the presence of new medium acid sites. The new medium acid sites are ascribed to the interaction between the zinc species and the intrinsic acid sites in the MHZSM-5 zeolites.[15] Otherwise, addition of zinc species in MHZSM-5(NC) (MZnZSM-5-2(NC)) without CTAB also results in the increase of medium acid sites and decrease of strong acid sites.

The type and concentration of Brønsted and Lewis acid sites for the HZSM-5, MHZSM-5, and MZnZSM-5-2 samples were determined by Py-IR, and the results are shown in Fig. 3. The absorbance peaks at 1545 and 1454 cm^{-1} are representative of Brønsted and Lewis acid sites, respectively.[36] Compared with HZSM-5, the two mesoporous samples have more Lewis acid sites and less Brønsted acid sites. Moreover, the incorporation of zinc into zeolite (MZnZSM-5-2) leads to the production of more Lewis acid sites, which is confirmed by the Py-IR adsorption peak at 1616 cm^{-1} assigned to Lewis acid sites.[37] The amounts of pyridine adsorbed on acid sites at different temperatures were calculated, and the resultsare listed in Table 3. The amounts of Brønsted and Lewis acid sites moderately decrease with the increase of adsorption temperature. For MHZSM-5 and MZnZSM-5-2, the ratios of the amount of Brønsted acid sites to Lewis acid sites (*B*/*L*) are

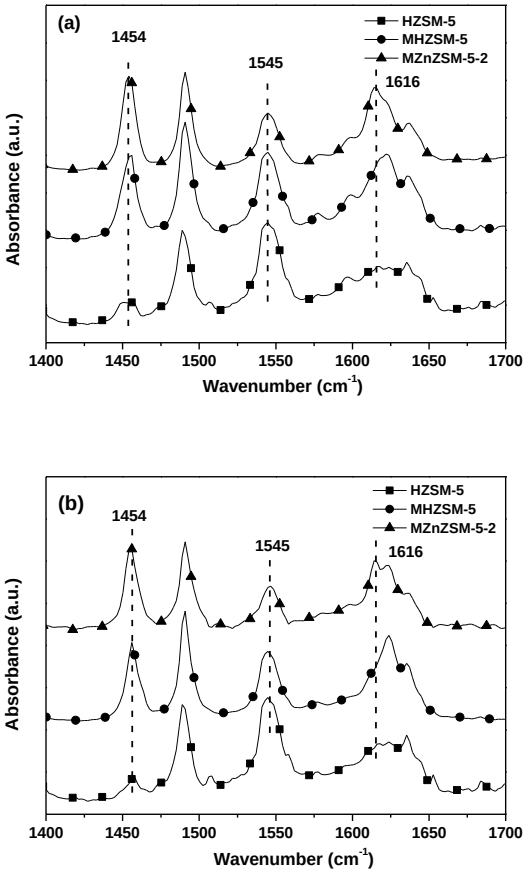

Fig. 3. Py-IR absorbance spectra of HZSM-5, MHZSM-5, and MZnZSM-5-2 samples at (a) 150 and (b) 350 °C.

substantially different from HZSM-5, which is attributed to the obvious decrease of Brønsted acid sites and increase of Lewis acid sites. It is concluded that treatment of HZSM-5 by desilication and reassembly (particularly for zinc-containing samples) can tune the acid site distribution on the catalyst surface, leading to the decrease of Brønsted acid sites and the production of more Lewis acid sites.

Table 3 Acid amounts of HZSM-5, MHZSM-5, and MZnZSM-5-2 determined by pyridine adsorption at 150, 250 and 350 °C.

Samples	150 °C (μmol/g)		*B/L*	250 °C (μmol/g)		*B/L*	350 °C (μmol/g)		*B/L*
	Brønsted	Lewis		Brønsted	Lewis		Brønsted	Lewis	
HZSM-5	493.1	57.5	8.58	460.6	46.2	9.98	344.6	37.2	9.26
MHZSM-5	336.1	173.3	1.94	288.2	143.4	2.01	201.2	118.2	1.70
MZnZSM-5-2	251.8	220.5	1.14	193.6	196.5	0.99	154.8	169.4	0.91

As reported in the literature, these Lewis acid sites can accelerate the dehydrogenation process, including hydride transfer and aromatization, and improve the selectivity for aromatic products.[38] Combined with the results of NH_3-TPD, it can be deduced that the decrease of acid strength of the mesoporous zeolites can be mainly attributed to acid redistribution on the catalyst surface. Moreover, most of the increased Lewis acid sites should be medium acid sites, and a small amount of Lewis acid sites is strong acid sites.

N_2 sorption measurements were carried out to quantify the porosity of the desilicated reassembled samples. The N_2 adsorption–desorption isotherms of the as-prepared samples are shown in Fig. 4(a). MHZSM-5 and MZnZSM-5-*x* exhibit high nitrogen uptake at relatively low pressure and a hysteresis loop at high relative pressure above P/P_0 = 0.4, indicating the coexistence of intrinsic micropores and mesopores generated by alkalinedesilication and CTAB-mediated reassembly. HZSM-5 shows a typical type I isotherm, which is characteristic for purely microporous zeolites. Fig. 4(b) shows the BJH pore-size distributions derived from the desorption branch of the as-prepared samples. Notably, MHZSM-5 shows two obvious pore-size distributions at 3–7 nm and 7–20 nm, which are assigned to mesopores obtained by CTAB reassembly involving dissolved species and the desilication process under alkaline conditions, respectively. This result is similar to that of previous report.[39] However, with increasing zinc content, the two obvious pore-size distributions at 3–7 nm and 7–20 nm change a pore-size range at 3–20 nm and the mesoporous amount gradually decreases. This indicates that the mesopores of MZnZSM-5-*x* become partly blocked with increasing zinc content. In the case of MHZSM-5(NC) and MZnZSM-5-2(NC), the mesopore distribution are wider (3–100 nm), which is different from the samples with addition of CTAB. This is consistent with the results of literature.[31] the textural properties of the as-prepared samples are summarized in Table 4. Compared with HZSM-5, the BET surface area, external surface area, and total volume of MHZSM-5 and MZnZSM-5-*x* are higher after alkaline desilication and CTAB reassembly, which is ascribed to the presence of mesopores in the samples. However, these textural parameters of MZnZSM-5-*x* gradually decrease withincreasing zinc content. As previously discussed, this is probably caused by the blockage of mesopores with increasing amount of zinc. Additionally, the micropore volume of MZnZSM-5-*x* decreases with increasing zinc content, suggesting that the addition of zinc also affects the crystallization of the microporous structure, which is in good agreement with the XRD results. That is, the

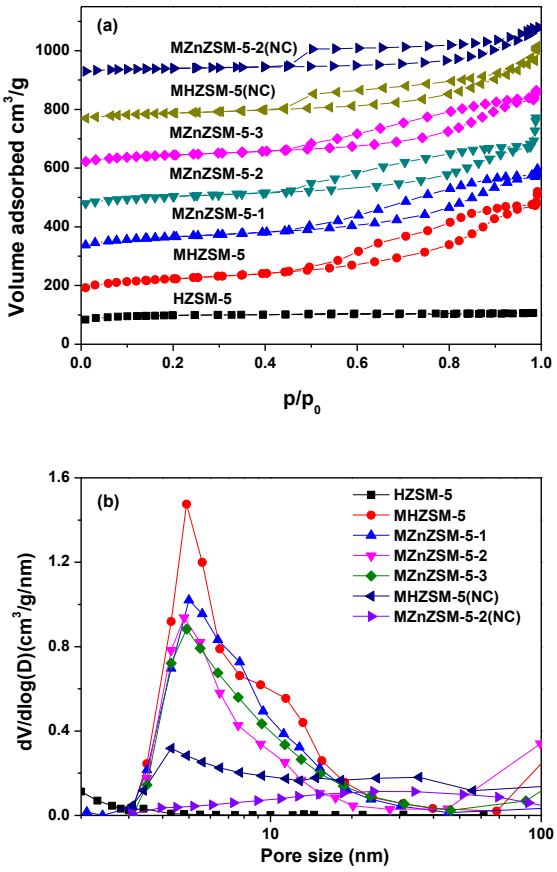

Fig. 4. (a) N_2 adsorption–desorption isotherms and (b) BJH pore-size distributions of HZSM-5, MHZSM-5, MZnZSM-5-x, MHZSM-5(NC) and MZnZSM-5-2(NC) samples.

micropore volume and intensity of the diffraction peaks are interrelated. Without CTAB, the surface area and volume of MHZSM-5(NC) are much lower than those of MHZSM-5, further confirming that the reassembly of CTAB in treatment process. Similar to MZnZSM-5-*x* samples, the external surface area and mesopore volume of MZnZSM-5-2(NC) further decrease, and meanwhile the microporous surface area and micropore volume reduce to 80 m^2/g and 0.032 cm^3/g respectively, which are also attributed to the blockage of mesopores and damage of microporous structure from the addition of zinc.

RSC Advances

ARTICLE

Table 4 Textural characteristics of the as-prepared samples.

Sample	S_{BET}[a] (m^2/g)	S_{exter}[b] (m^2/g)	S_{micro}[b] (m^2/g)	V_{total}[c] (cm^3/g)	V_{micro}[b] (cm^3/g)	V_{meso}[d] (cm^3/g)
HZSM-5	334	71	263	0.165	0.121	0.044
MHZSM-5	427	224	203	0.649	0.093	0.556
MZnZSM-5-1	401	197	204	0.536	0.093	0.443
MZnZSM-5-2	358	186	172	0.545	0.084	0.461
MZnZSM-5-3	328	161	167	0.486	0.076	0.410
MHZSM-5(NC)	301	134	167	0.487	0.077	0.410
MZnZSM-5-2(NC)	145	65	80	0.279	0.032	0.247

[a] S_{BET} was calculated by the BET method.
[b] S_{micro}, S_{exter} and V_{micro} were calculated by the *t*-plot method.
[c] V_{total} was calculated from the adsorption branch at $P/P_0 = 0.99$.
[d] V_{meso} was calculated from $V_{total} - V_{micro}$.

Fig. 5 shows SEM images of HZSM-5, MHZSM-5, MZnZSM-5-*x*, MHZSM-5(NC), MZnZSM-5-2(NC) and TEM image of MZnZSM-5-2. HZSM-5 has a typical hexagonal-shaped MFI crystal structure with crystal sizes of about 3–5 μm in length (Fig. 5(a)). The similar shape and crystal size of MHZSM-5 and HZSM-5 shows that desilication and CTAB-mediated reassembly have little effect on the morphology of zeolite (Fig. 5(b)). Moreover, the zinc content in the process of desilication and reassembly has no obvious influence on the structure of zeolite (Fig. 5(c)–(e)). However, both MHZSM-5(NC) and MZnZSM-5-2(NC) show severely fragmented crystal morphologies (Fig. 5(f) and (g)). This indicates that the dissolved structural units of zeolite did not reassemble well without CTAB, which is in agreement with their lower crystallinity. MZnZSM-5(NC) shows much lower crystallinity than MHZSM-5(NC) even though they have similar crystal morphologies. A possible reason is that the introduction of zinc species affects the crystallization of MZnZSM-5-2(NC) seriously. The TEM image of MZnZSM-5-2 reveals the presence of mesoporous channels (Fig. 5(h)). The mesopore size is in agreement with its pore-size distribution (Fig. 4(b)). Moreover, the macrocrystalline ZnO species are absent in MZnZSM-5-2 from the TEM image.

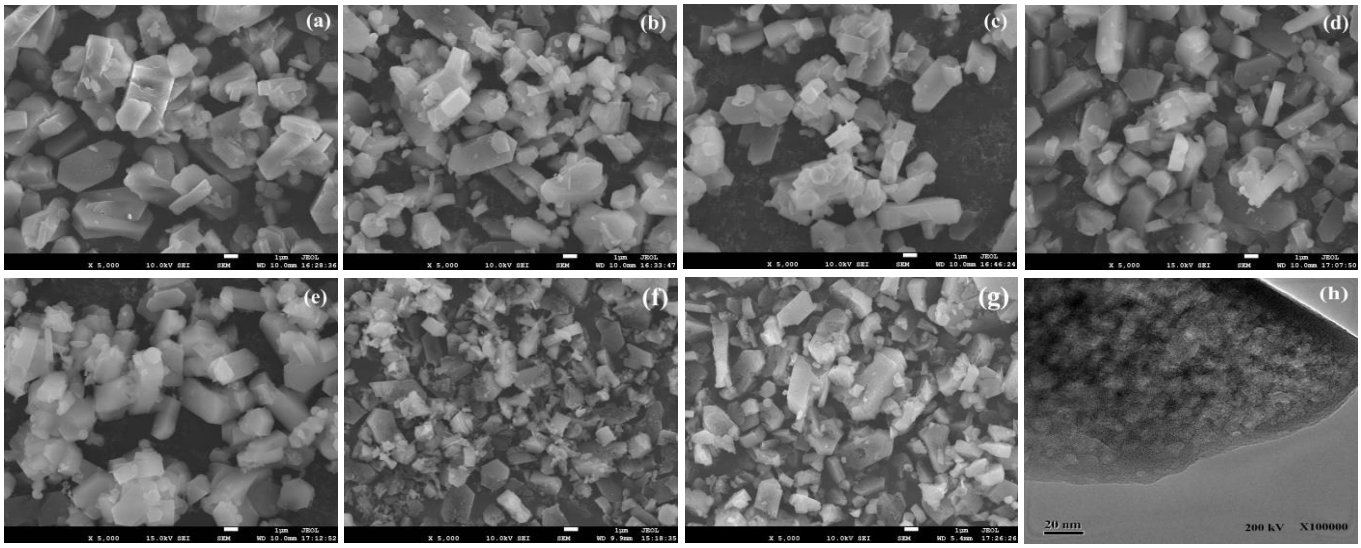

Fig. 5. SEM images of (a) HZSM-5, (b) MHZSM-5, (c) MZnZSM-5-1, (d) MZnZSM-5-2, (e) MZnZSM-5-3, (f) MHZSM-5(NC), (g) MZnZSM-5-2(NC) and TEM image of (h) MZnZSM-5-2.

RSC Advances

ARTICLE

The XPS results not only provide the state of surface zinc species in the Zn-containing zeolites, but also give the distribution of zinc species.[15] XPS analyses were performed to determine the chemical states of the surface Zn species in the samples. Fig. 6(a)–(c) shows the XPS spectra of Zn $2p_{3/2}$ for the MZnZSM-5-*x* samples. Clearly, the spectra of both MZnZSM-5-2 and MZnZSM-5-3 show the Zn $2p_{3/2}$ peak (Fig. 6(b,c)), whereas the peak is absent for MZnZSM-5-1 because of its considerably lower zinc content (Fig. 6(a)). By convoluting the XPS spectra of Zn $2p_{3/2}$, the spectra of MZnZSM-5-2 and MZnZSM-5-3 show two peaks with binding energies of about 1021.9 and 1023.0 eV (Fig. 6(b) and (c)). The low-intensity peak at 1021.9 eV indicates the presence of the ZnO species.[15,40] The peak at 1023.0 eV suggests the presence of zinc species having tighter interaction with the zeolite framework ($ZnOH^+$), which is linearly related to the enhanced selectivity for formation of aromatics in methanol aromatization.[15,41] Moreover, the intensity of the $ZnOH^+$ species peak of MZnZSM-5-3 is much higher than that of MZnZSM-5-2. The portion of surface $ZnOH^+$ species in MZnZSM-5-2 and MZnZSM-5-3 are about 87 % and 84 %, respectively. Though MZnZSM-5-3 shows a lower $ZnOH^+$ species proportion than MZnZSM-5-2, the Zn atom ratio in $ZnOH^+$ species of MZnZSM-5-3 (1.95 %) is higher than that of MZnZSM-5-2 (1.28 %). This indicates that MZnZSM-5-3 will probably have better selectivity for formation of aromatics in methanol aromatization.

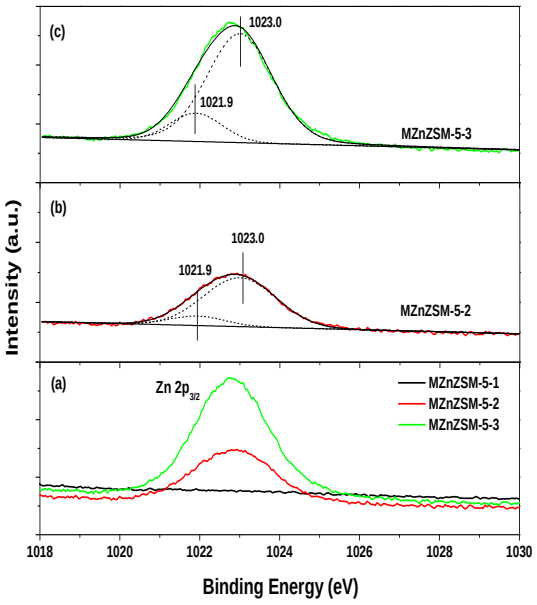

Fig. 6. (a) XPS spectra of Zn $2p_{3/2}$ for the MZnZSM-5-*x* samples. Deconvoluted spectra of (b) MZnZSM-5-2 and (c) MZnZSM-5-3.

Catalytic performance

Table 5 Product distribution for aromatization of methanol over different samples[a].

Catalyst	Selectivity (%)												
	CO_x[b]	C_1	C_2	C_3	C_4	C_5	C_6^+ aliph.	C_6H_6	C_7H_8	C_8H_9	C_9^+ arom.	BTX	Aromatics
HZSM-5	0.1	2.0	6.4	21.5	28.0	1.0	3.7	4.4	14.9	12.4	5.6	31.7	37.3
MHZSM-5	0.2	1.2	5.8	13.7	33.2	4.4	8.8	1.1	6.4	12.6	12.6	20.1	32.7
MZnZSM-5-1	0.2	1.2	6.2	13.2	30.5	4.0	8.7	1.4	8.0	14.2	12.5	23.6	36.1
MZnZSM-5-2	0.2	1.2	8.4	11.6	25.0	3.7	6.3	1.5	11.7	17.7	12.6	30.9	43.5
MZnZSM-5-3	0.1	1.1	8.7	10.3	22.3	3.7	7.0	1.4	12.6	19.2	13.5	33.2	46.7
MHZSM-5(NC)	0.1	1.3	4.7	15.5	33.9	4.8	9.4	1.6	8.6	15.7	4.4	25.9	30.3
MZnZSM-5-2(NC)[c]	1.2	4.8	36.3	10.1	16.4	5.5	1.3	0.1	1.9	4.9	1.1	6.9	8.0

[a]Reaction conditions: 430 °C, weight hourly space velocity (WHSV) = 1.7 h^{-1}, atmospheric pressure, 6 h. The conversion of methanol was 100% for all samples except for MZnZSM-5-2(NC).
[b]Including CO and CO_2.
[c]The conversion of methanol was 83.6%.

Table 5 shows the product distribution for aromatization of methanol over HZSM-5, MHZSM-5, and MZnZSM-5-*x* samples. The conversion of methanol was 100% over all of the samples except for MZnZSM-5-2(NC) (83.6%). Compared with HZSM-5, the selectivities for BTX and C_1, C_2, and C_3 hydrocarbon over MHZSM-5 are lower, and the selectivities for C_4^+ aliphatic hydrocarbons and C_9^+ aromatics are moderately higher. This suggests that the presence of mesoporous channels in the catalyst improves the selectivities for larger molecules and decreases the shape selectivities for BTX. With increasing zinc content in the samples, the BTX selectivity increases while the C_3 and C_4 selectivities decrease. It is believed that the increases in the selectivities for BTX and total aromatics are because of improved dehydrogenation and aromatization of low carbon number hydrocarbons owing to the increased number of Zn-Lewis acid sites.

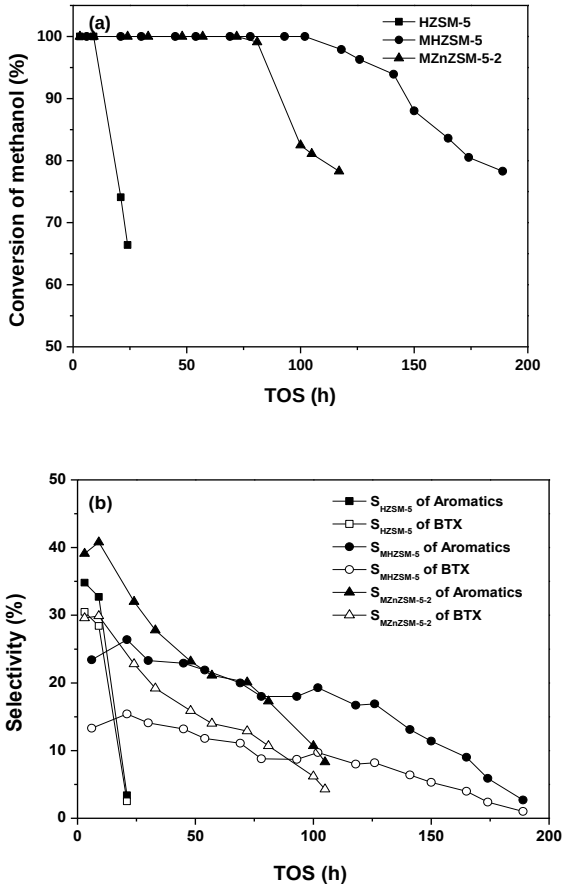

Fig. 7. (a) Conversion of methanol and (b) selectivity for BTX and aromatics formation versus time on-stream over HZSM-5, MHZSM-5, and MZnZSM-5-2 samples. Reaction conditions: 430 °C, atmospheric pressure, WHSV = 3.4 h^{-1}.

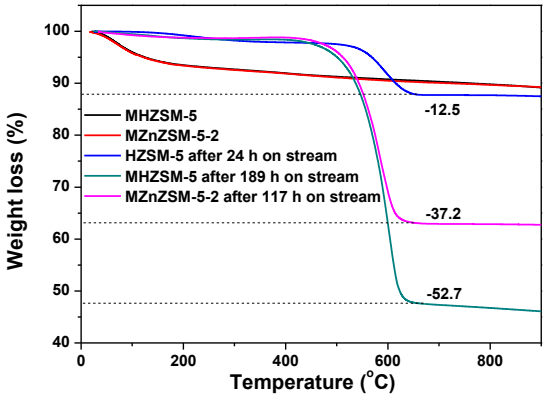

Fig. 8. TG profiles of fresh MHZSM-5 and MZnZSM-5-2 samples and HZSM-5, MHZSM-5 and MZnZSM-5-2 samples after the methanol aromatization reaction. The weight loss is representative of the amount of coke.

The conversion of methanol and the selectivity for aromatic formation versus time on-stream over HZSM-5, MHZSM-5, and MZnZSM-5-2 samples are shown in Fig. 7(a). MHZSM-5 and MZnZSM-5-2 show better catalyst stability compared with HZSM-5. Conversion of methanol over HZSM-5 rapidly decreases to 66.4% after 24 h on-stream, while those of both MHZSM-5 and MZnZSM-5-2 slowly decrease to about 78.3% after 189 h and 78.3% after 117 h on-stream, respectively. Additionally, the selectivities for aromatics and BTX for the HZSM-5, MHZSM-5, and MZnZSM-5-2 catalysts all decrease with time on-stream (Fig. 7(b)). It is inferred that coke gradually covers the active sites and blocks the pores of catalysts with time on-stream, so methanol conversion and BTX selectivity gradually decrease.

Fig. 8 shows TG profiles of fresh MHZSM-5 and MZnZSM-5-2 samples and HZSM-5, MHZSM-5 and MZnZSM-5-2 samples after the methanol aromatization reaction. It can be seen that both fresh MHZSM-5 and MZnZSM-5-2 show two weight losses below 200 °C and above 200 °C, and their TG profiles are almost coincident. The weight loss below 200 °C is attributed to the physical adsorbed water, and the slow weight loss above 200 °C is probably the small amount CTAB remained in the mesopores. HZSM-5 exhibits weight loss of 12.5% after 24 h on-stream, whereas MHZSM-5 and MZnZSM-5-2 show weight losses of 52.7% after 189 h and 37.2% after 117 h on-stream, respectively. Compared to fresh MHZSM-5 and MZnZSM-5-2, most of the weight losses of MHZSM-5 and MZnZSM-5-2 after the reaction are attributed to the coke, and only a small amount of weight losses are from CTAB remained in the mesopores. The weight loss per hour represents the average rate of coke formation. The average rates of coke formation on MHZSM-5 and MZnZSM-5-2 are 0.28% and 0.32% per hour, which are much lower than the coking rate of 0.52% per hour on the HZSM-5 catalyst. This is ascribed to the much higher mesopore volume and external surface area, as well as the fewer strong acid sites of MHZSM-5 and MZnZSM-5-2. Furthermore, MHZSM-5 has the much lower coke formation rate than MZnZSM-5-2 because of its higher external surface area and mesopore volume.

In this study, MHZSM-5 and MZnZSM-5-2 catalysts show the obviously higher catalytic stabilities than HZSM-5. The obviously improved long lifetimes of MHZSM-5 and MZnZSM-5-2 is mainly attributed to two aspects. On the one hand, mesoporous HZSM-5 and microporous HZSM-5 have the diverging pore systems. From the TEM image and textural properties, the mesoporous samples show the obvious intracrystalline mesopores and much larger mesopore volume and external surface area. In contrast, HZSM-5 exhibits extremely low mesopore volume from the intercrystalline mesopores and external surface area. Moreover, Ryoo and coworkers reported that coke is deposited on the external surfaces more than it is inside the micropores for microporous HZSM-5.[35] Recently, Schmidt *et al.* also reported that carbonaceous species accumulate and locate on the outer particle layers of microporous HZSM-5, and this coke layer blocks the active sites in the interior of catalyst causing poorer catalytic performance. On the contrary, mesoporous HZSM-5 zeolites show a homogeneous coke distribution from inside to outside of mesoporous zeolite particles and have less diffusion restraints, and therefore the active sites of the whole particle can contribute to the methanol conversion. Moreover, the larger external surface area and mesopore volume further enhance the capacity of coke.[42] Therefore, the mesoporous catalysts exhibit a lower inactivation rate. On the other hand, the mesoporous catalysts show the markedly decreased strong acid sites from NH_3-TPD. Usually, strong acid sites are active in methanol to hydrocarbon conversion.[43] Meanwhile, the strong acid sites are also the carbon centers. From the conversion of methanol and TG profiles, HZSM-5 with more strong acid sites shows weight loss of 12.5%, while the conversion of methanol rapidly decreases to 66.4% after 24 h on-stream. However, MHZSM-5 and MZnZSM-5-2 with fewer strong acid sites show weight losses of 52.7% and 37.2%, while the conversions of methanol slowly decrease to about 78.3% after 189 h and 78.3% after 117 h on-stream respectively. These results illustrate that MHZSM-5 and MZnZSM-5-2 possess the much longer catalytic lifetime and larger carbon capacity than HZSM-5. Therefore, the catalytic stability of catalyst mainly depends on the distribution and amount of coke, which are closely correlative with the structure and strong acid sites of catalyst.

In addition, MHZSM-5 shows the lower BTX selectivity than HZSM-5, which also is attributed to two aspects. For one thing, the number of strong acid sites of MHZSM-5 is evidently decreased due to the dissolution of silica framework, and these strong acid sites are active in the MTH reaction. For another thing, the channel selectivity of MHZSM-5 for BTX is poorer than HZSM-5 due to the presence of mesopores. On the contrary, the mesopores are favorable to enhance the selectivity of larger molecular aromatics. Table 5 reveals that the selectivity of C_9^+ aromatics over MHZSM-5 catalyst is much higher than that over HZSM-5. However, though MHZSM-5(NC) possesses a certain amount of mesopores, the selectivity of C_9^+ aromatics is still low. The possible reason is that the mesopore range of MHZSM-5(NC) without CTAB is much wider than that of MHZSM-5. For zinc-containing MZnZSM-5-x catalysts, the strong Brønsted acid sites are obviously reduced after the introduction of zinc species, and the amount of $ZnOH^+$ species is increased gradually with increasing zinc content. Brønsted acid sites in zeolites are essential for the formation of olefins from methanol, which then undergo dehydro-cyclooligomerization and hydrogen transfer reactions to generate aromatics and alkanes. Moreover, the BTX and aromatics selectivities are increased with increasing the amount of $ZnOH^+$ species from Table 5. Niu and coworkers proposed that there is a linear correlation between the amount of $ZnOH^+$ species and the selectivity to aromatics for MTA in the Zn/ZSM-5 catalysts. The introduction of zinc species causes a decrease of the strong acid sites, which is, however, compensated by the zinc metal centers with high activity for dehydrogenation and aromatization. [15] Song *et al.* proposed that the strong acid sites are necessary for the transformation of methanol, ethanol and olefins to aromatics. After poisoning of some strong acid sites, HZSM-5 shows much lower aromatization activity in MTA.[44] However, HGaMFI zeolites exhibit high aromatization activity due to the high dehydrogenation activity of metal Ga.[45] Xiao *et al.* also reported that the Brønsted acid sites and the strong Lewis acid sites generated by the $(GaO)^+$ species of Ga/HZSM-5 catalyst have a synergistic effect on propane aromatization.[46] Similar to MHZSM-5, the channel selectivity of zinc-containing MZnZSM-5-x for BTX is also poorer than that of HZSM-5, which is favorable to the formation of C_9^+ aromatics. In summary, the formation of aromatics from methanol over the Zn-containing MZnZSM-5-*x* catalysts is attributed to the synergy of the Brønsted acid sites, the Zn-Lewis acid sites and mesoporous channels.

Conclusions

A series of mesoporous MZnZSM-5-*x* zeolites with different zinc contents were prepared by simple one-step desilication and reassembly. The presence of CTAB improves crystallization of the zeolites (especially zinc-containing zeolites). MHZSM-5 and MZnZSM-5-*x* contain lower amounts of strong acid sites compared with HZSM-5, while the amount of medium acid sites of MHZSM-5 and MZnZSM-5-*x* obviously increased. With increasing zinc content, the crystallinity, external surface area, and mesopore volume of MZnZSM-5-*x* gradually decrease. The zinc species introduced during desilication and reassembly mainly concentrate on the surface of zeolites, and have tighter interaction with the zeolite framework ($ZnOH^+$). Moreover, the $ZnOH^+$ species is proportional to the amount of added zinc, and meanwhile $ZnOH^+$ acts as the active sites for the dehydrogenation of light hydrocarbons. Compared with HZSM-5, the BTX selectivity of MHZSM-5 remarkly reduces, and meanwhile the BTX selectivity of MZnZSM-5-*x* is higher than that of MHZSM-5, which is also increased with increasing zinc content. The formation of aromatics from methanol over the Zn-containing MZnZSM-5-*x* catalysts is attributed to the synergy of the strong Brønsted acid sites, the Zn-Lewis acid sites and mesoporous channels. The much improver catalytic stabilities of MHZSM-5 and MZnZSM-5-2 catalysts than HZSM-5 are attributed to their diverging pore systems and the decreased amount of strong acid sites.

Acknowledgments

Financial support from the Important Directed Program in the Chinese Academy of Science (KGCX2-YW-318-1) is gratefully acknowledged.

Notes and references

[1] M.A. Fahim, T.A. Alsahhaf and A. Elkilani, *Fundamentals of Petroleum Refining, The Netherlands*, 2010, 95–152.
[2] M. Stöcker, *Micropor. Mesopor. Mater.*, 1999, **29**, 3–48.
[3] J.F. Haw, W.G. Song, D.M. Marcus and J.B. Nicholas, *Acc. Chem. Res.,* 2003, **36**, 317–326.
[4] R. Barthos, T. Bansagi, T.S. Zakar and F. Solymosi, *J. Catal.*, 2007, **247**, 368–378.
[5] J. Kim, M. Choi and R. Ryoo, *J. Catal.*, 2010, **269**, 219–228.
[6] C.D. Chang, A.J. Silvestri, *J. Catal.*, 1977, **47**, 249–259.
[7] Y. Inoue, K. Nakashiro, Y. Ono, *Micropor. Mater.*, 1995, **4**, 379–383.
[8] T. Tian, W.Z. Zhai, Y.J. Sun, Y. Cui, Y.Y. Lu, F. Wei, *Mod. Chem. Ind.*, 2009, **29**, 55–58. In Chinese.
[9] H.A. Zaidi, K.K. Pant, *Catal. Today*, 2004, **96**, 155–160.
[10] H.A. Zaidi, K.K. Pant, *Ind. Eng. Chem. Res.*, 2008, **47**, 2970–2975.
[11] R. Barthos, T. Bánsági, T.S. Zakar, *F. Solymosi, J. Catal.*, 2007, **247**, 368–378.
[12] D. Freeman, R.P.K. Wells, G.J. Hutchings, *J. Catal.*, 2002, **205**, 358–365.
[13] Y. Ono, H. Adachi, Y. Senoda, J. Chem. Soc., *Faraday Trans. 1*, 1988, **84**, 1091–1099.
[14] Y. Ni, A. Sun, X. Wu, J. Hu, T. Li, G. Li, *Chin. J. Chem. Eng.*, 2011, **19(3)**, 439–445.
[15] X.J. Niu, J. Gao, Q. Miao, M. Dong, G.F. Wang, W.B Fan, Z.F. Qin and J.G. Wang, *Micropor. Mesopor. Mater.*, 2014, **197**, 252–261.
[16] Y. Ni, A. Sun, X. Wu, G. Hai, J. Hu, T. Li, G. Li, *Micropor. Mesopor. Mater.*, 2011, **143**, 435–442.
[17] C.J.H. Jacobsen, C. Madsen, J. Houzvicka, I. Schmidt and A. Carlsson, *J. Am. Chem. Soc.*, 2000, **122**, 7116–7117.
[18] Y.H. Chou, C.S. Cundy, A.A. Garforth and V.L. Zholobenko, *Micropor. Mesopor. Mater.*, 2006, **89**, 78–87.
[19] X. Wei, P.G. Smirniotis, *Micropor. Mesopor. Mater.*, 2006, **89**, 170–178.
[20] F.-S. Xiao, L. Wang, C. Yin, K. Lin, Y. Di, J. Li, R. Xu, D. Su, R. Schlögl, T. Yokoi and T. Tatsumi, *Angew. Chem. Int. Ed.*, 2006, **45**, 3090–3093.
[21] H. Zhu, Z. Liu, D. Kong, Y. Wang and Z. Xie, *J. Phys. Chem. C*, 2008, **112**, 17257–17264.
[22] H. Wang, T.J. Pinnavaia, *Angew. Chem. Int. Ed.*, 2006, **45**, 7603–7606.
[23] H. Zhu, Z. Liu, Y. Wang, D. Kong, X. Yuan and Z. Xie, *Chem. Mater.*, 2008, **20**, 1134–1139.
[24] S. ven Donk, A.H. Jansen, J.H. Bitter and K.P. de Jong, *Catal. Rev.*, 2003, **45**, 297–319.
[25] M. Ogura, S. Shinomiya, J. Tateno, Y. Nara, E. Kikuchi and M. Matsukata, *Chem. Lett.*, 2000, 882–883.
[26] S. Inagaki, M. Ogura, T. Inami, Y. Sasaki, E. Kikuchi and M. Matsukata, *Micropor. Mesopor. Mater.*, 2004, **74**, 163–170.
[27] Q. Tang, H. Xu, Y. Zheng, J. Wang, H. Li and J. Zhang, *Appl. Catal. A*, 2012, **413–414**, 36–42.
[28] V.V. Ordomsky, V.Y. Murzin, Y.V. Monakhova, Y.V. Zubavichus, E.E. Knyazeva, N.S. Nesterenko and I.I. Ivanova, *Micropor. Mesopor. Mater.*, 2007, **105**, 101–110.
[29] J. Garcia-Martinez, M. Johnson, J. Valla, K. Li and J.Y. Ying, *Catal. Sci. Technol.*, 2012, **2**, 987–994.
[30] W.C. Yoo, X. Zhang, M. Tsapatsis and A. Stein, *Micropor. Mesopor. Mater.*, 2012, **149**, 147–157.
[31] F. Schmidt, M. R. Lohe, B. Büchner, F. Giordanino, F. Bonino and S. Kaskel, *Micropor. Mesopor. Mater.*, 2013, **165**, 148–157.
[32] N. Al-Yassir, M.N. Akhtar, K. Ogunronbi and S. Al-Khattaf, *J. Mole. Cata. A: Chemical*, 2012, **360**, 1–15.
[33] J. Chen, Z. Feng, P. Ying, and C. Li, J. Phys. Chem. B 2004, **108**, 12669–12676.
[34] M. Niwa, N. Katada, M. Sawa, Y. Murakami, J. Phys. Chem., 1995, **99**, 8812–8816.
[35] J. Kim, M. Choi, R. Ryoo, *J. Catal.*, 2010, **269**, 219–228.
[36] H. Berndt, G. Lietz, B. Lücke and J. Völter, *Appl. Catal. A*, 1996, **146**, 351–363.
[37] Q. Yu, Y. Li, X. Meng, Q. Cui and C. Li, *Mater. Lett.*, 2014, **124**, 204–207.
[38] H. Mochizuki, T. Yokoi, H. Imai, S. Namba, J. N. Kondo and T. Tatsumi, *Appl. Catal. A*, 2012, **449**, 188–197.
[39] W.C. Yoo, X. Zhang, M. Tsapatsis and A. Stein, *Micropor. Mesopor. Mater.*, 2012, **149**, 147–157.
[40] N. Sapawe, A.A. Jalil, S. Triwahyono, R.N.R.A. Sah, N.W.C. Jusoh, N.H.H. Hairom and J. Efendi, *Applied Catalysis A: General*, 2013, **456**, 144–158.
[41] J. Chen, L. Zhang, H.M. Kang and F.X. Ding, *Chin. J. Catal.,* 2001, **22**, 229–232.
[42] Schmidt F, Hoffmann C, Giordanino F, Bordiga S, Simon P, Carrillo-Cabrera W and Kaskel S, *J. Catal.*, 2013, **307**, 238–245.
[43] S.M. Campbell, X.-Z. Jiang and R.F. Howe, *Micropor. Mesopor. Mater.*, 1999, **29**, 91–108.
[44] Y. Song, X. Zhu, S. Xie, Q. Wang, L. Xu, *Catal. Lett.*, 2004, **97**, 31–36.
[45] V.R. Choudhary, A.K. Kinage, *Zeolites*, 1995, **15**, 732–738.
[46] H. Xiao, J. Zhang, P. Wang, Z. Zhang , Q. Zhang, H. Xie, G. Yang, Y. Han and Y. Tan, *RSC Adv.*, 2015, **5**, 92222–92233.

Graphical abstract

Mesoporous ZnZSM-5 Zeolites Synthesized by One-Step Desilication and Reassembly: Durable Catalyst for Methanol Aromatization

Xiaoxing Wang, Junfeng Zhang,Tao Zhang, He Xiao, Faen Song, Yizhuo Han and Yisheng Tan*

Mesoporous ZnZSM-5 zeolite synthesized by simple alkaline desilication and CTAB-mediated reassembly shows obviously improved catalytic stability for methanol aromatization.